Magnetic order and electromagnon excitations in $DyMnO_3$ studied by neutron scattering experiments

T. Finger,[1] K. Binder,[1] Y. Sidis,[2] A. Maljuk,[3,4] D. N. Argyriou,[3,*] and M. Braden[1,†]

[1]*II. Physikalisches Institut, Universität zu Köln, Zülpicher Strasse 77, D-50937 Köln, Germany*

[2]*Laboratoire Léon Brillouin, CEA/CNRS, F-91191 Gif-sur-Yvette Cedex, France*

[3]*Helmholtz-Zentrum Berlin, Hahn-Meitner Platz 1, D-14109 Berlin, Germany*

[4]*Leibniz Institute for Solid State and Materials Research Dresden, Helmholtzstrasse 20, D-01069 Dresden, Germany*

(Received 21 October 2014; published 18 December 2014)

Magnetic order and excitations in multiferroic $DyMnO_3$ were studied by neutron scattering experiments using a single crystal prepared with an enriched ^{162}Dy isotope. The ordering of Mn moments exhibits pronounced hysteresis arising from the interplay between Mn and Dy magnetism, which has a strong impact on the ferroelectric polarization. The magnon dispersion resembles that reported for $TbMnO_3$. We identify the excitations at the magnetic zone center and near the zone boundary in the *b* direction, which can possess electromagnon character. The lowest frequency of the zone-center magnons is in good agreement with a signal in a recent optical measurement, so this mode can be identified as the electromagnon coupled by the same Dzyaloshinskii-Moriya interaction as the static multiferroic phase.

DOI: 10.1103/PhysRevB.90.224418 PACS number(s): 75.85.+t, 75.30.Ds, 75.47.Lx

I. INTRODUCTION

Strong magnetoelectric coupling may not only imply multiferroic order, i.e., a phase with coupled magnetic and ferroelectric order, but may also result in hybridized collective excitations of combined polar phonon and magnetic character, which are called electromagnons [1,2]. Such excitations may interact with the electromagnetic radiation through the electric and magnetic channels, opening the path for multichroism effects [3–5]. The fact that these effects can be controlled through the multiferroic state might become of great technical relevance. Through the application of moderate electric fields multiferroic domains can be easily manipulated [6–8], consequentially allowing one to switch the properties of reflected or transmitted electromagnetic radiation.

The understanding of the dynamic magnetoelectric effects, however, remains too limited. Following the discovery of the multiferroic phases in $REMnO_3$ [9–12], with *RE* being a rare-earth metal, the first evidence of electromagnon scattering was reported for this class of materials [13]. It seems intuitive to apply the same magnetoelectric coupling mechanism, which explains well the static multiferroic phases, to collective excitations [14]. In many of the recently discovered transition-metal-oxide-based multiferroics, ferroelectric polarization $\vec{P}$ can be explained by the model of inverse Dzyaloshinskii-Moriya (DM) coupling [15–17] with

$$\vec{P} \propto \vec{r}_{ij} \times (\vec{S}_i \times \vec{S}_j). \quad (1)$$

Here $\vec{r}_{ij}$ is the distance vector between coupled spins $\vec{S}_i$ and $\vec{S}_j$. The inverse DM coupling yields only weak electromagnon scattering due to the small coupling coefficients arising from spin-orbit coupling. Electromagnon scattering in $REMnO_3$, however, is quite strong, and the main part of it cannot be modified by rotating the static cycloidal order [18]. While in $TbMnO_3$ the multiferroic phase is characterized by a magnetic cycloid in the *bc* plane in zero magnetic field [19–22], this plane flops to the *ab* plane [23] upon the application of magnetic fields along the *a* or the *b* direction as well as in the case of other REs. In contrast, the strong electromagnon response always appears for electric fields along the *a* direction [18,24]. A large variety of electromagnon measurements using optical or dielectric techniques was reported [13,18,24–36], along with several theories to explain the strong electromagnon scattering along *a* [18,37–41]. In addition, inelastic neutron scattering gives insight into the magnetic character of these modes [42–44].

Taking $TbMnO_3$ as the prototypical material for the new class of multiferroics, one may identify at least three electromagnon contributions in optical and dielectric studies [28,31,33]: the strongest response is at 7.5 meV, followed by a signal at 2.7 meV (at 12 K). In addition a third electromagnon response occurs at the low energy of 1.5 meV [31] that is more difficult to detect with optical methods due to its low energy and due to its small signal strength. For the contribution at the highest energy Valdés Aguilar *et al.* [18] presented a convincing explanation based on a modulation of the symmetric exchange, which can be much stronger than that of the antisymmetric contributions. The structural distortion associated with the rotation of the MnO_6 octahedrons around the *c* axis generates strong coupling between a collective displacement of the planar oxygen ions against the Mn ions and a magnetic mode near the zone boundary of the magnetic zone [18] (see discussion below). It is widely accepted that this exchange-striction mechanism explains the strong electromagnon response at high energy. In addition the static mechanism must also be relevant [14] and explains the electromagnon signal at the lowest energies [13,31,33,35,36], which, however, possesses much lower spectral weight. The intermediate electromagnon, however, still needs further studies, and a signal at even higher energies is most likely not related to intrinsic electromagnon scattering [28].

*Present address: European Spallation Source, S-22100 Lund, Sweden.

†braden@ph2.uni-koeln.de

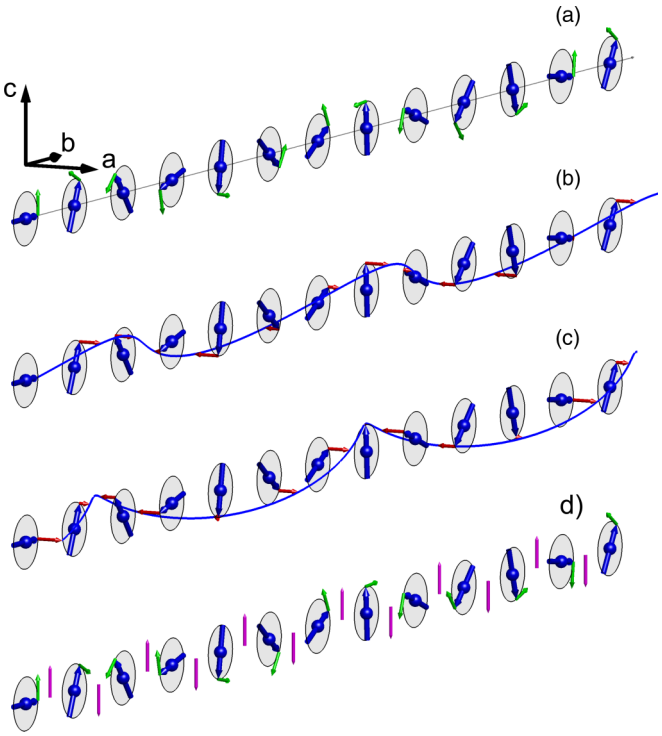

FIG. 1. (Color online) Illustration of polarization patterns of several magnon modes which are relevant for the discussion of electromagnons in $DyMnO_3$. In all parts the static cycloid is shown by large blue arrows rotating in the cycloid plane indicated by the shaded circles. The propagation vector of the modulation in b corresponds to that in $DyMnO_3$ with two Mn atoms per layer and unit cell. (a) The pattern of the phason mode at the magnetic zone center. The frozen-in oscillating displacements of the spins are indicated by the small green arrows. Adapting the inverse Dzyaloshinskii-Moriya interaction described by Eq. (1) does not result in an oscillating polarization because the cross product $(\vec{S}_i \times \vec{S}_j)$ is constant. (b) The CRM associated with the rotation of the entire cycloid around the b direction. In this mode the spin cross product and thus the electric polarization rotate around b so that there is an oscillating polarization along a which can couple with electromagnetic radiation with $\vec{E}$ parallel to a. (c) The HM in which the spiral plane rotates around the c axis, modifying the character of the spiral from a pure cycloid to a partially helical one. Applying Eq. (1) will yield only a quadratic coupling with the electric polarization. (d) The polarization of the mode polarized within the cycloid plane (b,c plane) appearing at the propagation vector with the k component $k_{\mathrm{elm-str}} = 1 - k_{\mathrm{inc}} = 0.64$. This mode gains a strong oscillating electric polarization through the exchange striction mechanism. In the static cycloid the scalar product $\vec{S}_i \cdot \vec{S}_j$ is constant; its momentous deviation from the average value is indicated by the vertical magenta bars.

Comprehensive inelastic neutron scattering experiments in the cycloidal phases of $TbMnO_3$ yield a microscopic characterization of the magnon excitations and strong support for the picture described above [42–45]. First, the modes near the magnetic zone boundary in the b direction indeed exhibit energies at which the strongest electromagnon scattering is found in optical studies. Three magnon modes can be identified at the magnetic zone center, e.g., at $\vec{Q} = (0\,0.28\,1)$ or $\vec{Q} = (2\,0.28\,1)$, and are illustrated in Figs. 1(a)– 1(c). One mode can be associated with the oscillation of the phase of the cycloid, i.e., the phason. This mode cannot induce any electromagnon character because the vector product of the neighboring spins and thus the induced polarization do not vary [see Eq. (1) and Fig. 1(a)]. Two other modes are characterized by the rotation of the cycloid plane around the b and c directions, respectively [14,42]. Neglecting any anisotropies, the mode for the rotation around the b direction [see Fig. 1(b)] can be considered to be the Goldstone mode of the multiferroic transition and should possess zero energy (thus being massless) [43]. Applying Eq. (1), this mode is associated with the rotation of the ferroelectric polarization around b which corresponds to an oscillation of the polarization in the a direction. This mode thus exhibits electromagnon character [14,42] and can be measured with optical techniques for $\vec{E}(\omega) \parallel \vec{a}$. By analyzing the possible anisotropy energies Senff *et al.* [43] deduced that this rotational mode of the cycloid should be the zone-center magnon with lower but still finite energy, and indeed, the few spectroscopic studies capable of examining the dielectric response at low enough energies did find excitations at the corresponding energies [13,31,33,35,36]. The other a polarized zone-center magnon changes the character of the cycloid to a partial helical character [see Fig. 1(c)]. In order to differentiate between these two modes we will label the first the cycloid rotation mode [CRM; see Fig. 1(b)] and the second the helical mode [HM; see Fig. 1(c)]. The CRM corresponds to the proposal in Ref. [14]. It is tempting to compare the intermediate electromagnon scattering in $TbMnO_3$ with the HM as, indeed, the frequencies match well. However, the strength of the dielectric signal does not agree with the character of this mode. The electromagnon weight could arise through mixing with other modes [18,38], but it seems more likely that other magnon modes cause this intermediate electromagnon response through the more effective exchange striction mechanism [38–40]. Due to the flat dispersion between (001) and the magnetic Bragg point many magnon modes possess energies in this range.

While the electromagnon response in the various $RE\mathrm{MnO_3}$ compounds has been studied with different dielectric or optical techniques, so far only multiferroic $TbMnO_3$ has been studied by inelastic neutron scattering because of the high neutron absorption of natural Sm, Eu, Gd, and Dy. In this work we used Dy with enriched ^{162}Dy isotope content to grow a large crystal that is suitable for inelastic experiments. The sequence of magnetic transitions in $DyMnO_3$ is similar to that in $TbMnO_3$ [19–22], with a first transition to a longitudinal spin-density wave along b at 38 K followed by the development of cycloidal order in the bc plane at 18 K and the onset of ordering of Dy moments below 10 K [46–48]. However, the interplay between RE and Mn magnetism seems to be stronger in the Dy compound, which is assumed to contribute to enhanced ferroelectric polarization [47]. Indeed, we find pronounced hysteresis effects in the Dy as well as in the Mn ordering as a function of temperature. The magnetic excitations and their dispersion also strongly resemble the findings for $TbMnO_3$, which somehow contrasts with the different electromagnon response in $DyMnO_3$ reported by dielectric studies.

II. EXPERIMENT

A large single crystal of $DyMnO_3$ was grown using the traveling floating-zone technique in an image furnace. The feed rod

was synthesized with a ^{162}Dy isotope content enriched to 90% while a seed crystal with natural Dy was used. The crystal was characterized by superconducting quantum interference device (SQUID) measurements which can identify the ordering of Dy moments at 5.4(3) and 7.1(3) K upon cooling and heating, respectively [49]. Measurements of specific heat allow one to determine three ordering temperatures by the maxima in c_p/T at 5.7(3), 18.8(3), and 38.2(3) K [49], in perfect agreement with previously reported measurements [46–48] and the neutron diffraction experiments described below.

Elastic and inelastic neutron scattering experiments were performed with the cold triple-axis spectrometer 4F2 ($k_f = 1.55$ Å^{-1}) and with the thermal triple-axis spectrometer 1T ($k_f = 2.66$ Å^{-1}) at the Orphée reactor in Saclay. At 4F2 a double monochromator and an analyzer using the (002) reflection of pyrolytic graphite (PG) were utilized, and a Be filter was set between the sample and the analyzer in order to suppress higher-order contaminations. On 1T a PG monochromator, a PG analyzer, and a PG filter were used. Two cylindrical crystals about 4 mm thick and $\sim$ 5 mm in diameter were coaligned in the [010]/[001] scattering geometry for the 4F2 experiment; for the structural studies on 1T a smaller single piece of the same growth was mounted. Throughout the paper we use reduced lattice units to address scattering vectors referring to the orthorhombic lattice in the setting of $Pbnm$ with $a = 5.27$ Å, $b = 5.83$ Å, and $c = 7.35$ Å. The sample was cooled using an orange-type liquid-helium cryostat and a closed-cycle refrigerator on 4F2 and 1T, respectively.

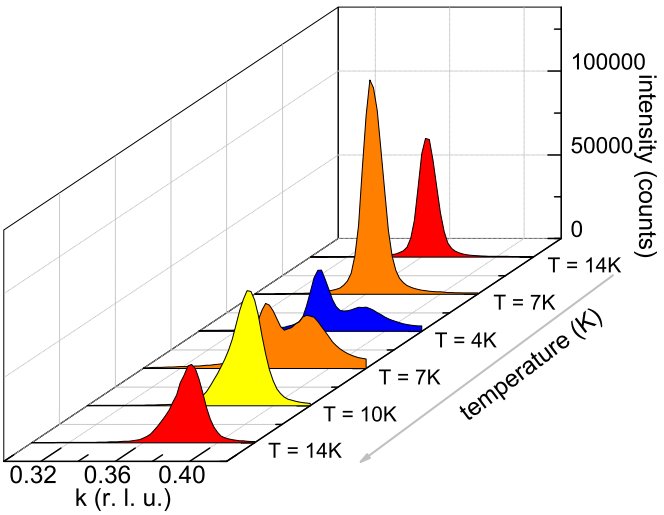

FIG. 2. (Color online) Temperature dependence of the magnetic $(0k1)$ reflection measured from an isotopically enriched $DyMnO_3$ single crystal. Data were collected on the 4F2 spectrometer upon cooling and heating (counting time of ~60 s); note the different peak positions observed even far above the ordering temperature of Dy moments.

III. RESULTS AND DISCUSSION

A. Magnetic ordering in $DyMnO_3$

The sequence of magnetic transitions in $DyMnO_3$ has been studied using resonant and nonresonant x-ray techniques [46–48]. These studies give access to only the intrinsic ordering of Dy moments and the structural distortions accompanying the ordering of Mn moments. In contrast, the ordering of Mn moments has not been studied so far. The emergence of magnetic order in $DyMnO_3$ is qualitatively similar to that of $TbMnO_3$, but the Dy moments seem to possess a stronger impact even far above the onset of full order of these moments. Upon cooling, ordering of Mn moments sets in at $T_N = 38.2$ K, with an incommensurate modulation along the b direction described by the propagation vector (0 0.36 0). We study the magnetic ordering near $\vec{Q} = (0\,0.36\,1)$, which takes into account the antiferromagnetic coupling along the c direction. The temperature dependence of the wavelength of the magnetic modulation was previously studied via the coupled lattice modulation of half the wave length corresponding to the doubled pitch of the propagation vector. Strempfer *et al.* found a pronounced hysteresis between cooling and heating cycles [48]. With our neutron diffraction experiment we may directly analyze the ordering of the Mn moments, and we can confirm the strong difference between cooling and heating cycles (see Fig. 2, which displays data obtained with the large sample on 4F2). In the first cooling from room temperature we find a peak centered near (0 0.363 1) which strongly increases in intensity upon cooling to 7 K. Upon further cooling below the onset of magnetic order of Dy moments, which corresponds to a different propagation vector of (0 0.5 0), the signal of the Mn moments seems to split, with an additional contribution appearing at (0 0.39 1). Reheating to 7 K, however, does not yield the initial peak, but the additional contribution becomes enhanced and finally dominant at 10 K. Even heating to 14 K does not yield the initial arrangement, although this temperature is well above the suppression of Dy moment order, which disappears upon heating at 7.1 K, as observed in the SQUID data. In order to further elucidate this complex hysteresis, two full cooling and heating cycles were recorded on the 1T spectrometer which yielded identical results, but only one cycle is shown in Fig. 3. The scans across the signals arising from the Mn moments were fitted by one or two Lorentzian peaks, yielding the results shown in Fig. 4.

Figure 3 demonstrates the pronounced hysteresis of the Mn spin order between cooling and heating which can be perfectly explained by the coupling of the Dy and Mn magnetism and by a strong coupling of the anisotropic Dy ions with the lattice. Upon cooling we find the propagation vector near (0 0.36 1) and an onset of Bragg scattering at $T_N = 38.2$ K (see Fig. 4). Cooling to about 25 K results in little variation in the modulation but in a strong increase in intensity, which, however, suddenly drops at further cooling, accompanied by a step in the modulation vector. The second magnetic transition associated with the onset of ferroelectric order is visible as a kink in the temperature dependence of the magnetic modulation [see inset of Fig. 4(b)], which stays constant at lower temperatures. The intensity of the magnetic signal at (0 0.363 1) sharply increases upon further cooling, indicating a stronger modulation of Dy moments with the same period as that of the Mn moments. This additional intensity is suppressed at the magnetic ordering of Dy moments near 5 K [see inset of Fig. 4(a)] because Dy moments order at a distinct propagation vector of (0 0.5 0). The onset of the Dy moment order is also visible in the broad diffuse scattering accompanying

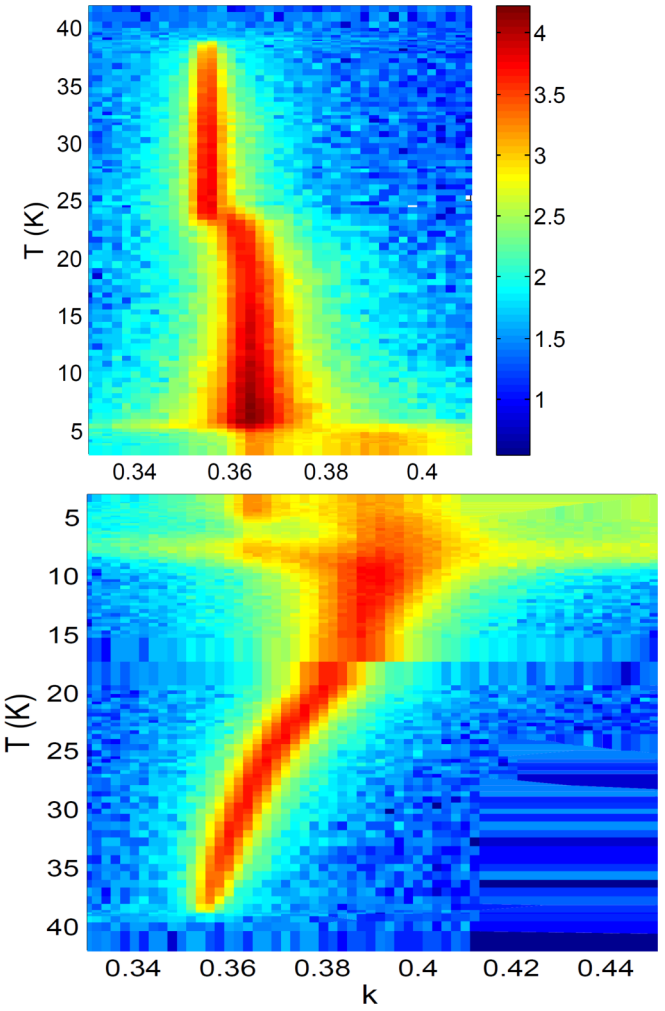

FIG. 3. (Color online) Temperature dependence of elastic magnetic scattering in $DyMnO_3$ at $(0k1)$ studied on the 1T spectrometer upon (top) cooling and (bottom) heating. At fixed temperatures the scattering intensity was recorded by scanning along $(0k1)$. The color coding corresponds to a logarithmic scale for a counting time of about 15 s; note that the lower scans extend to larger k values.

the transition that extends even beyond the wave vector of the Mn moments. Concomitantly, the Mn order becomes unpinned and exhibits a double signal. The additional Mn moment modulation appears at $(0 \sim 0.39\ 1)$. This modulation seems to be responsible for the signal observed in resonant x-ray diffraction at the Dy edge near (0 2.9 3), which is just the combination of the intrinsic Dy order and the latter modulation of the Mn moments. The two values observed for the modulation of Mn moments most likely arise from strong and minor contributions of Dy moments to the two modulations, respectively. These results qualitatively agree with the modulations found at the doubled wave vectors with x-ray techniques [46–48], but the isotope-enriched crystal seems to exhibit slightly smaller incommensurabilities.

The bottom panel of Fig. 3 shows the following heating sequence. In the temperature range to 7 K there is some variation in the pitch of the additional Mn signal which becomes dominant upon heating. Again, the loss of Dy order near 7.1 K [see inset of Fig. 4(a)] is visible in the broad

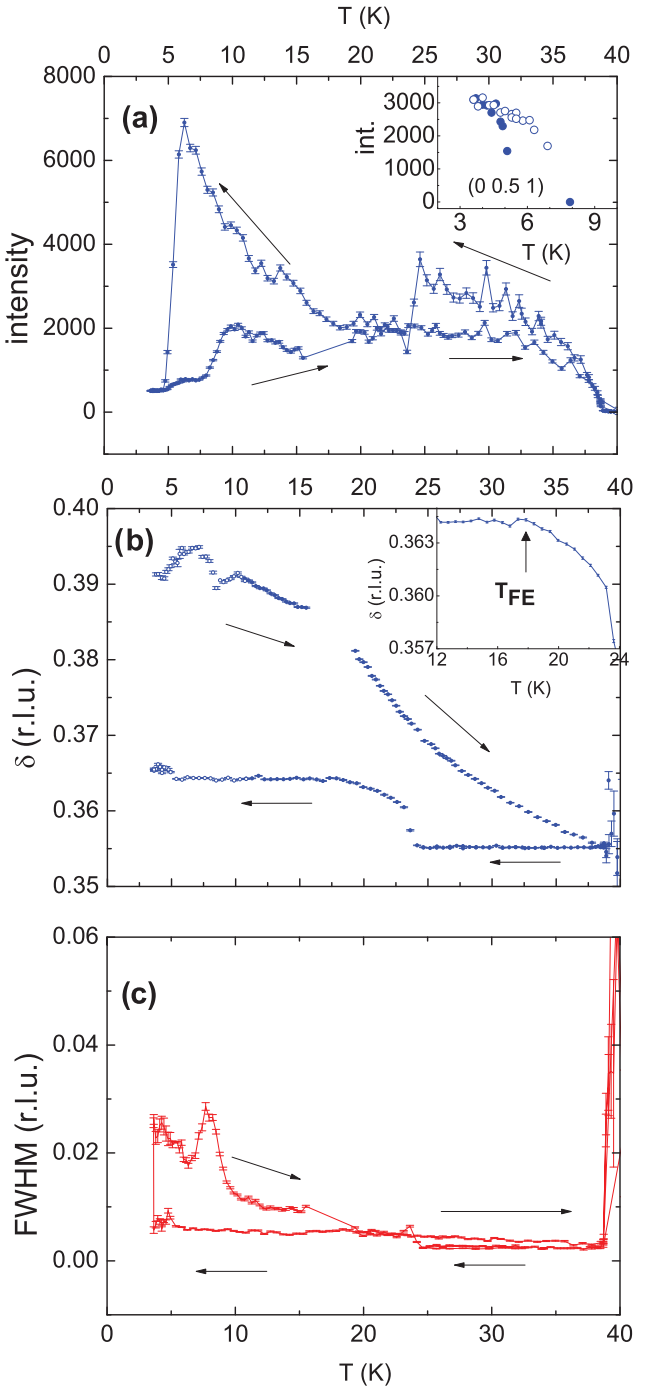

FIG. 4. (Color online) Temperature dependence of elastic magnetic $(0k1)$ scattering in $DyMnO_3$ studied on the 1T spectrometer upon cooling and heating. The $(0k1)$ scans shown in Fig. 3 were fitted by one or two Lorentzian peak profiles (see Fig. 3). (a) The peak intensity (height) of the strongest peak as a function of temperature; the inset displays the height of the (0 0.5 1) peak that is associated with the ordering of Dy moments upon cooling (solid circles) and heating (open circles). (b) The incommensurate pitch (peak position) of the strongest signal; at low temperatures (open circles) the measured profiles were fitted with two Lorentzians. The inset displays an enlargement of the temperature range near 18 K corresponding to the onset of ferroelectric order. (c) The temperature dependence of the FWHM of the fitted peak profiles, which senses the impact of the Dy ordering.

intensity distribution. Above this transition, only the Mn signal at larger k remains, and it exhibits an intensity similar to that of the initial signal upon first cooling, indicating again a strong contribution of the Dy moments. However, note that the modulation vector of the Mn order at 10 K is different for cooling and heating, which explains the hysteretic effects in the ferroelectric polarization [10].

The hysteresis of the Mn moment magnetism in this broad temperature range is remarkable. It arises from two effects: the intrinsic hysteresis of the Dy order and the hysteresis of the coupling of Dy and Mn moments with differing preferred propagation vectors. The latter results in the two k components of the propagation vectors of the Mn ordering of 0.36 and 0.39. Upon cooling the Dy order cannot induce the transformation of the Mn ordering to larger values as it occurs at too low temperature. Upon heating, the Dy order shifts to 7.1 K, and this extended temperature range seems sufficient to fully transform the Mn order to the larger k component. In order to recover the initial scheme of Mn moment ordering one has to heat up the crystal close to T_N. The modulation of the Mn order only smoothly decreases with heating towards the initial values due to the continuous depinning and due to the melting of Dy moments. Figure 4(c) shows the temperature dependence of the widths of the fitted peak profiles at (0 ∼ 0.4 1) arising from the ordering of Mn moments. Above T_N the magnetic scattering of course becomes very broad, but also near the onset and near the disappearance of the Dy order the Mn magnetism is heavily perturbed. In addition, the interplay seems to imply a finite width of the Mn signal in almost the entire temperature range, and just after the first cooling to slightly below T_N sharp magnetic peaks exist.

Resuming these elastic studies, we find a close coupling between the magnetism of Dy and Mn moments with very pronounced pinning effects. These hysteresis and pinning effects have a clear impact on the ferroelectric polarization. The pyrocurrent measurements by Goto *et al.* [10] were taken upon heating; they show a huge difference between two runs recorded after cooling down to 2 and 7 K, respectively, which reflects the essential differences in the Mn ordering observed upon cooling and heating shown in Figs. 2 and 3. Apparently, the longer-wavelength magnetic modulation appearing upon cooling results in an up to ∼50% larger ferroelectric polarization. A strong hysteresis is also observed in the dielectric constant along c measured on a thin film of $DyMnO_3$ [50]. In this dielectric measurement cooling and heating results fall together only above the Néel temperature, resembling our findings for the modulation vector of Mn moments.

B. Magnetic excitations in $DyMnO_3$

Magnetic excitations were studied on the 4F2 spectrometer using cold neutrons, $k = 1.55$ Å^{-1}. The main part of these measurements was performed at $T = 14$ K in the multiferroic phase [11,49] but well above the ordering of Dy moments. Nevertheless, Dy moments are already sizably polarized at this temperature, which implies a more complex magnon dispersion. Data were taken after cooling the sample to only 10 K. The crystal-field excitations in $DyMnO_3$ have not yet been studied using inelastic neutron scattering, and an infrared experiment detected only one crystal-field excitation at 22.9 meV, which lies far above the energy range studied here [51]. Lower crystal-field energies were just calculated to amount to 5.7 and 15.7 meV [51]. At the lower of these values we do not find evidence for a strong crystal-field scattering. However, the same experiment reports a splitting of the Kramer's doublet degeneracy by an interaction between Mn and Dy moments of 3.7 meV [51], which might agree with a weak $\vec{Q}$-independent signal in our scans (see Fig. 5), but for an unambiguous interpretation further studies are needed.

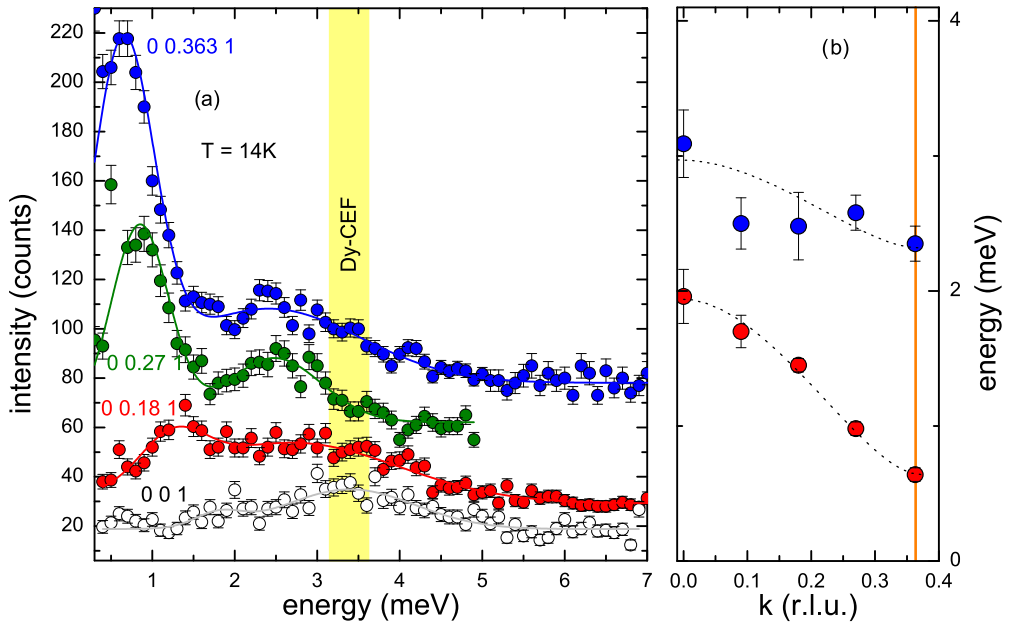

FIG. 5. (Color online) (a) Constant $\vec{Q}$ scans to determine the low-energy magnetic excitations between $\vec{Q} = (0\,0.363\,1)$ and (0 0 1) and dispersion. Slightly above an energy of 3 meV some signal may arise from a Dy crystal-field excitation of the lifting of Kramer's doublet degeneracy. (b) The flat dispersion in this part of the Brillouin zone.

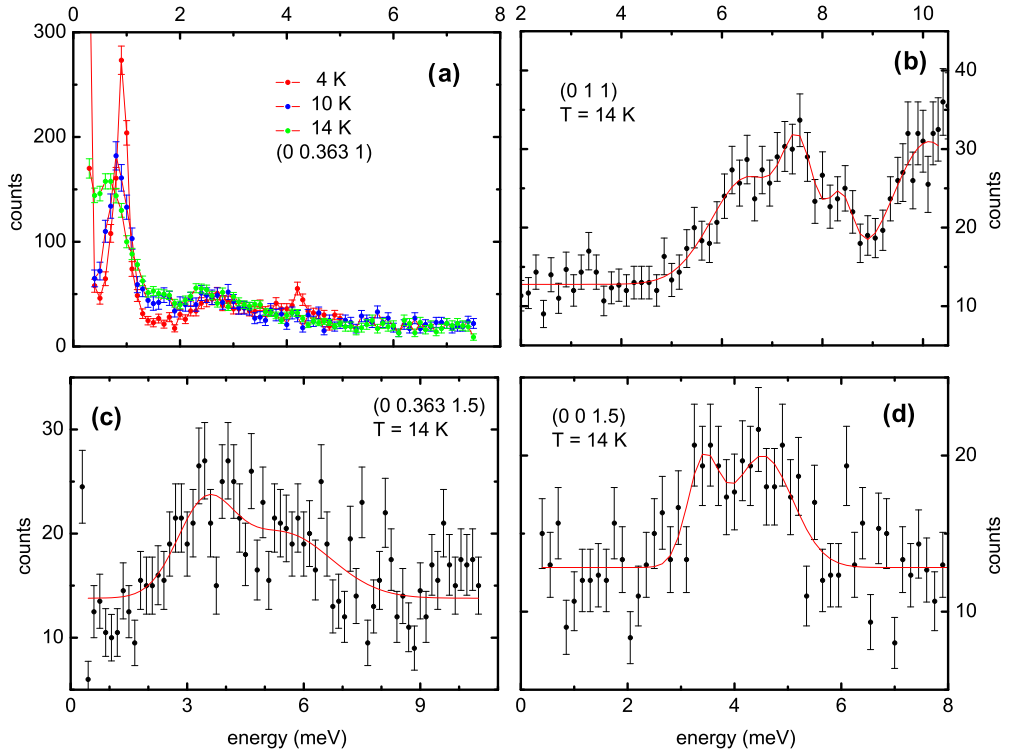

FIG. 6. (Color online) Constant $\vec{Q}$ scans taken at various point in the Brillouin zone to establish the magnon dispersion in $DyMnO_3$: (a) magnetic zone center, (b) end point of the dispersion in the b direction, and the zone boundary in the c direction (c) with and (d) without the incommensurate modulation along b.

The dispersive features discussed in the following cannot be attributed to Dy crystal-field excitations.

In view of the discussion of electromagnons, magnetic excitations at the zone center, i.e., taken at the magnetic Bragg points, are the most important, as these modes may couple with infinite wavelength structural distortions even in the harmonic case. Data taken at $\vec{Q} = (0\,0.363\,1)$ and other scattering vectors towards $\vec{Q} = (001)$ are shown in Fig. 5. At the magnetic zone center one may recognize a low-energy mode at 0.8 meV and another one near 2.3 meV. At this scattering vector modes polarized in the a direction fully contribute, while a mode polarized in the c direction is strongly suppressed. Note that, in general, neutron scattering only senses the magnetic components polarized perpendicular to the scattering vector [52]. It thus appears reasonable to identify the two observed modes with the a polarized modes arising from the rotations of the cycloid planes [42], CRM and HM [see Figs. 1(b) and 1(c)]. Furthermore, the observed frequencies agree with those reported for $TbMnO_3$ at a slightly higher temperature: energy of HM at 2.5 meV and energy of CRM at 1.1 meV at $T = 17$ K in $TbMnO_3$. Also the rather flat dispersion between the magnetic zone center and (001), which can be discerned for at least two branches, resembles the behavior in $TbMnO_3$. The phason mode, which contributes little to the data in Fig. 5, must possess a much smaller energy at the magnetic zone center. Both modes visible in Fig. 5 exhibit widths larger than what can be explained by the resolution (FWHM ~ 0.2 meV). This could be a consequence of the anharmonic folding discussed in Ref. [38].

Due to the less favorable scattering conditions with the small sample only the dispersion along the b direction and the zone boundary along c could be studied. The scans taken at the latter positions, (0 0.363 1.5) and (0 0 1.5), indicate a double signal near 4 meV (see Fig. 6), which again agrees with the dispersion reported for $TbMnO_3$. In this direction only the antiferromagnetic coupling along the c direction intervenes, which amounts to about $J_{AFM} = -0.5$ meV and which is little reduced between $LaMnO_3$ [53] and $TbMnO_3$ [43,45] and between $TbMnO_3$ and $DyMnO_3$.

The total dispersion along b ranging from $\vec{Q} = (001)$ and the magnetic Bragg point to the boundary at $\vec{Q} = (011)$ is shown in Fig. 7. The color plot displays the raw data and circles show the dispersion of the maxima obtained by fitting Gaussian intensity distributions. As for $TbMnO_3$ a split dispersion consisting of at least two or three branches can be followed across the entire zone, reaching energies of 6 to 8 meV at the zone boundary [see Fig. 6(b)], where the signal at higher energy seems to arise from a phonon. This suggests that the ferromagnetic interaction between nearest neighbors in the ab planes J_{FM} is little renormalized when passing from the Tb compound to the Dy compound, in agreement with the small difference in the ionic radii [43]. The main difference in the magnon dispersion arises from the enhanced frustration by the next-nearest-neighbor interaction along b, $J_{NNN} = -\eta J_{FM}$, which results in a larger value of the incommensurate modulation vector in $DyMnO_3$, $q_k = 0.36$ instead of 0.28 in $TbMnO_3$. In $DyMnO_3$ the interaction ratio η amounts to 1.15, compared with the value of 0.78 in $TbMnO_3$.

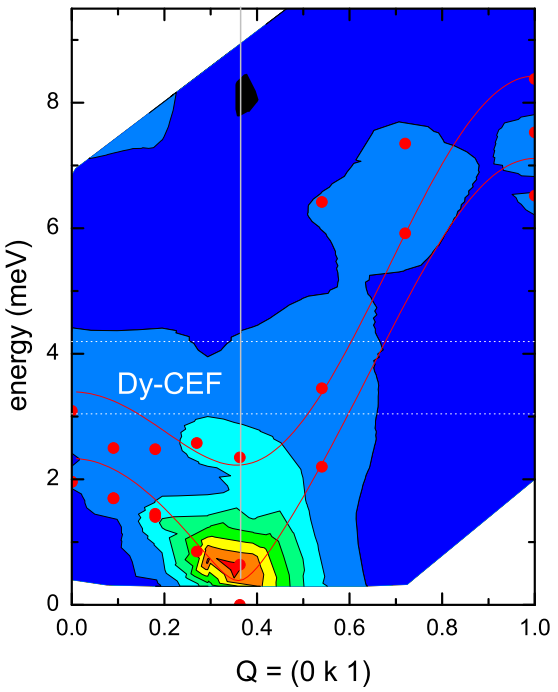

FIG. 7. (Color online) Dispersion of magnetic excitations along the b direction shown as a color contour plot of the scattered intensities. The lines denote the spin-wave dispersion calculated with linear theory as described in Ref. [43]. Parameters were $J_{\mathrm{FM}} = 0.12$ meV (0.14 meV), $J_{\mathrm{AFM}} = -0.4$ meV (-0.35 meV), and $\Lambda = 0.19$ meV (0.4 meV) for the lower (upper) curve; red dots denote peak positions determined by fitting Gaussians to the measured scans.

This enhanced frustration is in full agreement with the stronger structural distortion arising from the slightly smaller ionic radius in $DyMnO_3$. Further parameters needed to describe the dispersion are the antiferromagnetic exchange in the c direction J_{AFM}, the single-ion anisotropy term Λ, and the spin value $S = 2$ for Mn^{3+}. The simple spin-only Hamiltonian of the magnetic interaction is given by

$$\mathcal{H} = -\sum_{i,j} J_{i,j}\vec{S}_i \cdot \vec{S}_j - \Lambda \sum_i S_i^{z2}, \qquad (2)$$

where the sum only contains the nearest neighbors in the a,b planes J_{FM}, the nearest neighbors parallel to the c direction J_{AFM}, and the next-nearest neighbors in the planes J_{NNN}. Besides a significant change for η, only slight modifications are needed to describe the magnon dispersion in $TbMnO_3$ and $DyMnO_3$ (see Fig. 7).

Most interesting are the zone-center magnons as potential candidates for electromagnon modes. The temperature dependence of the two a polarized modes taken from the data in Fig. 6(a) is shown in Fig. 8. Both modes harden upon cooling, as expected. The energy of the lowest mode, which can be assigned to the CRM, perfectly agrees with the low-energy electromagnon signal detected recently in a terahertz (THz) radiation experiment [5]. As first proposed in Ref. [14], the rotation of the entire cycloid results in an electromagnon mode based on the same magnetoelectric DM coupling as the static multiferroic phase, but the dielectric oscillator strength of this electromagnon mode is small.

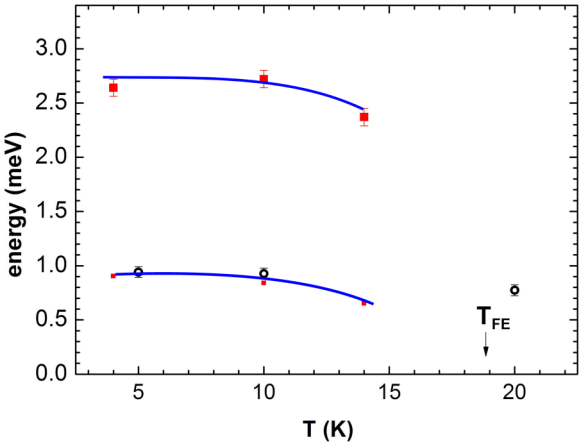

FIG. 8. (Color online) Temperature dependence of electromagnons in $DyMnO_3$. The inelastic neutron scattering results (red squares) are compared with those of spectroscopic measurements [5] (black circles) for the lowest mode. Lines are guides to the eye.

The higher zone-center mode near 2.5 meV, assigned to the HM, can be compared with electromagnon scattering observed in THz spectroscopy (see Ref. [26]). However, the largest peak in the THz radiation experiment (tracing ϵ_2) clearly exhibits a lower energy than the zone-center magnon; for example, at $T = 14$ K the optical peak appears at $\sim$1.7 meV, well below the magnon at 2.38(8) meV. The HM is not expected to exhibit strong polarization as the coupling between magnetic structure and polarization is quadratic. The intermediate-energy electromagnon scattering constitutes the strongest electromagnon signal in $DyMnO_3$ when tracing ϵ_2 [26], but considering the oscillator strength, both signals are comparable. In contrast, the high-energy signal clearly dominates in $TbMnO_3$ [28]. A mechanism other than the weak inverse DM interaction must be responsible for the intermediate optical signal. It has been proposed that the exchange striction mechanism combined with some backfolding of magnons is responsible for this strong low-energy scattering [38]. Indeed, the branches connecting the magnetic zone center to $\vec{Q} = (001)$ are quite flat [see Fig. 5(b)], giving support for such a picture; however, this flat branch lies significantly above the energy of the THz radiation signal [26].

In $DyMnO_3$, the electromagnon signal found in spectroscopic studies at the highest energy appears at $\sim$6 meV at 14 K, but this signal forms only a shoulder in ϵ_2 for $DyMnO_3$. Following the proposal of Valdés Aguilar *et al.*, this electromagnon arises from the exchange striction mechanism and a magnetic arrangement that benefits from an alternation of the magnetic exchange in the b direction [18]. The static arrangement in a $-\uparrow-\uparrow-\downarrow-\downarrow-$ structure (labeled E type in $REMO_3$ perovskites) couples to an alternation of enhancement and reduction of the ferromagnetic interaction in the bonds. This can be seen in the structure $-\uparrow-J_{\mathrm{FM}}^{+}-\uparrow-J_{\mathrm{FM}}^{-}-\downarrow-J_{\mathrm{FM}}^{+}-\downarrow-J_{\mathrm{FM}}^{-}-\uparrow-$in which parallel moments benefit from stronger ferromagnetic interaction. In a static cycloid with incommensurate modulation such an oscillating arrangement is not realized for the zone-boundary magnon of the orthorhombic structure but for the magnon with a k component of the wave vector of $k_{\mathrm{elm-str}} = 1 - k_{\mathrm{inc}} = 0.637$. This mode

is illustrated in Fig. 1(d), which also indicates the variation of the scalar product of neighboring spin, which alternates. A magnon energy at this k value of the b dispersion indeed amounts to 6 meV, in good agreement with the spectroscopic data (see Fig. 7). The fact that there is good agreement at quite different energies in $DyMnO_3$ and $TbMnO_3$ (for Tb this mode appears at 7.5 meV [28,43]) gives strong support for the exchange striction mechanism. The difference in the energies in $DyMnO_3$ and $TbMnO_3$ arises mainly from the different incommensurate pitch and its impact on $k_{\mathrm{elm-str}}$. It has been proposed that the strong low-energy peak in the optical response of $DyMnO_3$ and similar $REMnO_3$ compounds arises from strong backfolding of the magnon dispersion partially due to the local rotation of the magnetic anisotropy [38]. The measured dispersion, however, does not support fully such an interpretation as the strong backfolding effects cannot be observed between (0 0.36 1) and (011), although the dispersion is flat between (0 0.36 1) and (001) (see Figs. 5 and 7). Further efforts are needed to fully understand the reasons for the strong electromagnon response slightly below the frequency of the HM.

IV. CONCLUSIONS

The study of the magnetic ordering confirms the close coupling between Mn and Dy moments, which results in remarkable hysteresis effects. The intrinsic hysteresis of the Dy moment ordering and the depinning of the incommensurate Mn modulation result in a complex hysteretic behavior which perfectly corresponds to the reported hysteresis in the temperature dependence of the ferroelectric and dielectric properties.

The comparison of inelastic neutron scattering studies of the magnon dispersion in $DyMnO_3$ with previously reported spectroscopical measurements [5,26] helps identify the electromagnon modes. The high-energy optical signal perfectly fits with the energy of the magnon mode that is expected to strongly couple via the exchange striction mode. Its energy is significantly lower than that of the corresponding mode in $TbMnO_3$, mainly due to the enhanced value of the incommensurate modulation. The zone-boundary magnon energies differ much less between $DyMnO_3$ and $TbMnO_3$, indicating similarly strong nearest-neighbor ferromagnetic interactions. With regard to the electromagnon excitation at the lowest energy, there is good agreement between the dielectric studies and our neutron scattering experiments. This mode can be identified as the cycloid rotation mode which gets its electromagnon weight from the same inverse Dzyaloshinskii-Moriya mechanism as the static multiferroic order. Again, this agrees with the observations for $TbMnO_3$ [43]. With regard to the intermediate electromagnon signal, however, there is no agreement between the spectroscopical studies and the zone-center magnons sensed by neutron scattering. This finding is in contrast to the reports for $TbMnO_3$. The strong spectral weight observed near 2 meV in the optical studies on $DyMnO_3$ must possess a different origin that is eventually related to the backfolding of magnon branches. Indeed, the magnon dispersion seems to be quite flat between $(0q_{\mathrm{inc}}1)$ and (001).

ACKNOWLEDGMENT

This work was supported by the Deutsche Forschungsgemeinschaft through Sonderforschungsbereich 608 and Contract No. AR 613/1-1.

[1] V. G. Bar'yakhtar and I. E. Chupis, Sov. Phys. - Solid State **10**, 2818 (1969).
[2] G. A. Smolenskii and I. E. Chupis, Sov. Phys. Usp. **25**, 475 (1982).
[3] I. Kézsmárki, N. Kida, H. Murakawa, S. Bordács, Y. Onose, and Y. Tokura, Phys. Rev. Lett. **106**, 057403 (2011).
[4] S. Bordács, I. Kézsmárki, D. Szaller, L. Demkó, N. Kida, H. Murakawa, Y. Onose, R. Shimano, T. Room, U. Nagel, S. Miyahara, N. Furukawa, and Y. Tokura, Nat. Phys. **8**, 734 (2012).
[5] A. Shuvaev, V. Dziom, A. Pimenov, M. Schiebl, A. A. Mukhin, A. C. Komarek, T. Finger, M. Braden, and A. Pimenov, Phys. Rev. Lett. **111**, 227201 (2013).
[6] Y. Yamasaki, S. Miyasaka, Y. Kaneko, J.-P. He, T. Arima, and Y. Tokura, Phys. Rev. Lett. **96**, 207204 (2006).
[7] T. Hoffmann, P. Thielen, P. Becker, L. Bohatý, and M. Fiebig, Phys. Rev. B **84**, 184404 (2011).
[8] M. Baum, J. Leist, Th. Finger, K. Schmalzl, A. Hiess, L. P. Regnault, P. Becker, L. Bohatý, G. Eckold, and M. Braden, Phys. Rev. B **89**, 144406 (2014).
[9] T. Kimura, S. Ishihara, H. Shintani, T. Arima, K. Takahashi, K. Ishizaka, and Y. Tokura, Nature (London) **426**, 55 (2003).
[10] T. Goto, T. Kimura, G. Lawes, A. P. Ramirez, and Y. Tokura, Phys. Rev. Lett. **92**, 257201 (2004).
[11] T. Kimura, G. Lawes, T. Goto, Y. Tokura, and A. P. Ramirez, Phys. Rev. B **71**, 224425 (2005).
[12] S.-W. Cheong and M. Mostovoy, Nat. Mater. **6**, 13 (2007).
[13] A. Pimenov, A. Mukhin, V. Ivanov, V. Travkin, A. Balbashov, and A. Loidl, Nat. Phys. **2**, 97 (2006).
[14] H. Katsura, A. V. Balatsky, and N. Nagaosa, Phys. Rev. Lett. **98**, 027203 (2007).
[15] H. Katsura, N. Nagaosa, and A. V. Balatsky, Phys. Rev. Lett. **95**, 057205 (2005).
[16] M. Mostovoy, Phys. Rev. Lett. **96**, 067601 (2006).
[17] I. A. Sergienko and E. Dagotto, Phys. Rev. B **73**, 094434 (2006).
[18] R. Valdés Aguilar, M. Mostovoy, A. B. Sushkov, C. L. Zhang, Y. J. Choi, S.-W. Cheong, and H. D. Drew, Phys. Rev. Lett. **102**, 047203 (2009).
[19] S. Quezel, F. Tcheou, J. Rossat-Mignod, G. Quezel, and E. Roudaut, Physica B **86–88**, 916 (1977).
[20] J. Blasco, C. Ritter, J. García, J. M. de Teresa, J. Pérez-Cacho, and M. R. Ibarra, Phys. Rev. B **62**, 5609 (2000).
[21] M. Kenzelmann, A. B. Harris, S. Jonas, C. Broholm, J. Schefer, S. B. Kim, C. L. Zhang, S.-W. Cheong, O. P. Vajk, and J. W. Lynn, Phys. Rev. Lett. **95**, 087206 (2005).
[22] R. Kajimoto, H. Yoshizawa, H. Shintani, T. Kimura, and Y. Tokura, Phys. Rev. B **70**, 012401 (2004).

[23] N. Aliouane, K. Schmalzl, D. Senff, A. Maljuk, K. Prokes, M. Braden, and D. N. Argyriou, Phys. Rev. Lett. **102**, 207205 (2009).
[24] R. Valdés Aguilar, A. B. Sushkov, C. L. Zhang, Y. J. Choi, S.-W. Cheong, and H. D. Drew, Phys. Rev. B **76**, 060404(R) (2007).
[25] A. Pimenov, T. Rudolf, F. Mayr, A. Loidl, A. A. Mukhin, and A. M. Balbashov, Phys. Rev. B **74**, 100403(R) (2006).
[26] N. Kida, Y. Ikebe, Y. Takahashi, J. P. He, Y. Kaneko, Y. Yamasaki, R. Shimano, T. Arima, N. Nagaosa, and Y. Tokura, Phys. Rev. B **78**, 104414 (2008).
[27] A. B. Sushkov, R. Valdés Aguilar, S. Park, S.-W. Cheong, and H. D. Drew, Phys. Rev. Lett. **98**, 027202 (2007).
[28] Y. Takahashi, N. Kida, Y. Yamasaki, J. Fujioka, T. Arima, R. Shimano, S. Miyahara, M. Mochizuki, N. Furukawa, and Y. Tokura, Phys. Rev. Lett. **101**, 187201 (2008).
[29] J. S. Lee, N. Kida, S. Miyahara, Y. Takahashi, Y. Yamasaki, R. Shimano, N. Furukawa, and Y. Tokura, Phys. Rev. B **79**, 180403 (2009).
[30] Y. Takahashi, Y. Yamasaki, N. Kida, Y. Kaneko, T. Arima, R. Shimano, and Y. Tokura, Phys. Rev. B **79**, 214431 (2009).
[31] A. Pimenov, A. Shuvaev, A. Loidl, F. Schrettle, A. A. Mukhin, V. D. Travkin, V. Yu. Ivanov, and A. M. Balbashov, Phys. Rev. Lett. **102**, 107203 (2009).
[32] Y. Takahashi, Sh. Ishiwata, Sh. Miyahara, Y. Kaneko, N. Furukawa, Y. Taguchi, R. Shimano, and Y. Tokura, Phys. Rev. B **81**, 100413(R) (2010).
[33] A. M. Shuvaev, V. D. Travkin, V. Y. Ivanov, A. A. Mukhin, and A. Pimenov, Phys. Rev. Lett. **104**, 097202 (2010).
[34] P. Rovillain, M. Cazayous, Y. Gallais, A. Sacuto, M.-A. Measson, and H. Sakata, Phys. Rev. B **81**, 054428 (2010).
[35] Y. Takahashi, R. Shimano, Y. Kaneko, H. Murakawa, and Y. Tokura, Nat. Phys. **8**, 121 (2012).
[36] Y. Takahashi, Y. Yamasaki, and Y. Tokura, Phys. Rev. Lett. **111**, 037204 (2013).
[37] A. Cano, Phys. Rev. B **80**, 180416(R) (2009).
[38] M. Mochizuki, N. Furukawa, and N. Nagaosa, Phys. Rev. Lett. **104**, 177206 (2010).
[39] M. P. V. Stenberg and R. de Sousa, Phys. Rev. B **80**, 094419 (2009).
[40] M. P. V. Stenberg and R. Sousa, Phys. Rev. B **85**, 104412 (2012).
[41] T. Hasegawa, S. Miyahara, and N. Furukawa, J. Phys. Conf. Ser. **200**, 012053 (2010).
[42] D. Senff, P. Link, K. Hradil, A. Hiess, L. P. Regnault, Y. Sidis, N. Aliouane, D. N. Argyriou, and M. Braden, Phys. Rev. Lett. **98**, 137206 (2007).
[43] D. Senff, N. Aliouane, D. N. Argyriou, A. Hiess, L. P. Regnault, P. Link, K. Hradil, Y. Sidis, and M. Braden, J. Phys. Condens. Matter **20**, 434212 (2008).
[44] D. Senff, P. Link, N. Aliouane, D. N. Argyriou, and M. Braden, Phys. Rev. B **77**, 174419 (2008).
[45] R. Kajimoto, H. Mochizuki, H. Yoshizawa, H. Shintani, T. Kimura, and Y. Tokura, J. Phys. Soc. Jpn. **74**, 2430 (2005).
[46] R. Feyerherm, E. Dudzik, N. Aliouane, and D. N. Argyriou, Phys. Rev. B **73**, 180401(R) (2006).
[47] O. Prokhnenko, R. Feyerherm, E. Dudzik, S. Landsgesell, N. Aliouane, L. C. Chapon, and D. N. Argyriou, Phys. Rev. Lett. **98**, 057206 (2007).
[48] J. Strempfer, B. Bohnenbuck, M. Mostovoy, N. Aliouane, D. N. Argyriou, F. Schrettle, J. Hemberger, A. Krimmel, and M. v. Zimmermann, Phys. Rev. B **75**, 212402 (2007).
[49] T. Cronert, Diploma thesis, University of Cologne, 2014.
[50] Ch. Lu, S. Dong, Z. Xia, H. Luo, Z. Yan, H. Wang, Z. Tian, S. Yuan, T. Wu, and J. Liu, Sci. Rep. **3**, 3374 (2013).
[51] S. Jandl, S. Mansouri, A. A. Mukhin, V. Yu Balbashov, and M. M. Gospodino, J. Magn. Magn. Mater. **323**, 1104 (2011).
[52] W. Marshall and S. W. Lovesey, *Theory of Thermal Neutron Scattering* (Clarendon, Oxford, 1971).
[53] F. Moussa, M. Hennion, J. Rodríguez-Carvajal, H. Moudden, L. Pinsard, and A. Revcolevschi, Phys. Rev. B **54**, 15149 (1996).